Porosity evolution during heating of copper made from powder by friction extrusion

Xiaolong Ma , Xiao Li , Gayaneh Petrossian , Angel Ortiz , Mageshwari Komarasamy , Scott Whalen , Glenn Grant , Suveen Mathaudhu , Nicole Overman

PII: S2589-1529(22)00028-X
DOI: https://doi.org/10.1016/j.mtla.2022.101341
Reference: MTLA 101341

To appear in: *Materialia*

Received date: 22 September 2021
Accepted date: 20 January 2022

Please cite this article as: Xiaolong Ma , Xiao Li , Gayaneh Petrossian , Angel Ortiz , Mageshwari Komarasamy , Scott Whalen , Glenn Grant , Suveen Mathaudhu , Nicole Overman , Porosity evolution during heating of copper made from powder by friction extrusion, *Materialia* (2022), doi: https://doi.org/10.1016/j.mtla.2022.101341

Porosity evolution during heating of copper made from powder by friction extrusion

Xiaolong Ma[1,*], Xiao Li[1], Gayaneh Petrossian[1], Angel Ortiz[1], Mageshwari Komarasamy[1], Scott Whalen[1], Glenn Grant[1], Suveen Mathaudhu[1, 2], Nicole Overman[1,]

[1]Energy and Environment Directorate, Pacific Northwest National Laboratory, Richland, WA, 99352, USA

[2]Metallurgical and Materials Engineering, Colorado School of Mines, Golden, CO, 80401, USA

[*]**Corresponding author:** Dr. Xiaolong Ma, Pacific Northwest National Laboratory, United States, E-mail: xiaolong.ma@pnnl.gov;xma4@ncsu.edu

Graphical Abstract

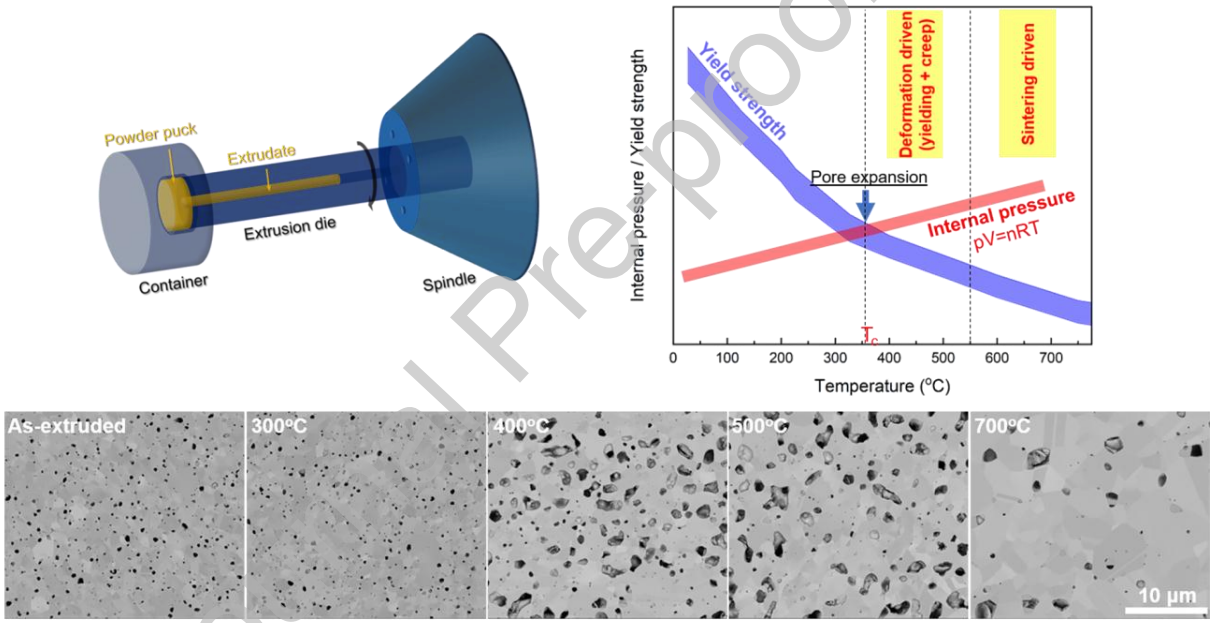

Abstract

Friction extrusion was used to compact and extrude solid copper rod from feedstock powders. Following extrusion, considerable porosity was observed throughout the extrudate cross section due to the entrained porosity in the feedstock material and the extrusion process. The thermal stability of the extrudate was investigated via a series of heat treatments. Porosity evolution exhibited three distinct stages—an unchanged plateau (0°C–300°C) followed by an abrupt increase (400°C–500°C) and ultimately a reduction, as the temperature increases (>500°C). The peak porosity measured was ~25%. The underlying driving force for pore evolution is described as the competition between the internal pore pressure, material strength, and sintering kinetics, as a function of temperature. The observed porosity evolution and driving force are not expected to be limited to copper. Thus, this manuscript reveals an important consideration regarding the microstructure thermal stability as advanced manufacturing methods involving direct powder extrusion are explored.

Keywords: Copper, Porosity, Thermal Stability, Extrusion, Consolidation

1. Introduction

For structural applications, the pore is a double-edged sword when present in the microstructures of metallic materials. Its presence, whether an advantage or a liability, often depends on the volume fraction. When metals have a large volume of pores, i.e., metallic foams [1,2], attractiveness comes in the form of a low-density material capable of high mechanical energy absorption efficiency and damping capacity [1,3]. On the other hand, when pores are localized imperfections in an overall low-porosity metal matrix, they usually act as stress concentrators and deteriorate mechanical properties, especially fatigue performance [4,5]. Manipulating porosity, by foaming (to gain high porosity) or consolidating (to eliminate pores), has achieved great success in conventional manufacturing by using different mechanisms for the pore evolution. For example, driven by the reduction of interfacial energy, sintering has been employed to fabricate consolidated products with minimized porosity by high-temperature heating of powders [6]. In contrast, Kearns et al. and other researchers took advantage of the long-time creep to fabricate highly porous materials by annealing the gas-filled powders for long durations to deliberately expand the pores [7,8].

Porosity evolution and manipulation in powder-based advanced manufacturing is still a subject of ongoing research. Hojjatzadeh et al. revealed that in laser powder bed fusion, pore motion is driven by the thermocapillary force and can be controlled by the temperature-gradient induced by laser [9]. Tammas-Williams et al. found that tiny remnant pores (less than 5 μm in diameter) in additively manufactured titanium components can regrow during heat treatment even after hot isostatically pressing, thereby highlighting the role of entrapped gas in pores [10]. Understanding of porosity evolution in materials processed by powder extrusion, another variant in advanced manufacturing through solid-state processing [11], remains relatively inadequate. Powder extrusion has distinctive characteristics that could uniquely affect pore evolution. For example, solid-state processing renders deformation stresses and material flow during consolidation [12], so changes in the state of stress could add another layer of complexity in deciphering the porosity evolution post heat treatment.

In this study, we investigate porosity in copper wire/rod made by friction extrusion and its evolution during post-extrusion heating at different temperatures. Microstructure characteristics and mechanical performance in different regimes ranging from 25°C to 700°C are explored to gain insights into the pore evolution as a function of heating temperature after extrusion. The underlying driving forces for the observed evolution and their implications on microstructural engineering are also discussed.

2. Materials and Methods

Two types of powders were used in this study. Powder A (99.5% purity), porous and with a powder size of 150–420 μm, was employed for the major study. Powder B (99.7% purity), pore-free and with a powder size of <40 μm, was extruded for a comparison to discern the source for the extrudate porosity. The powders of ~42 g were carefully weighed and filled into an H13 billet container with an inner diameter of 25.4 mm and pre-compacted into a puck under a hydraulic press at a pressure level of 170 MPa. The compacted powder was friction-extruded in a horizontal configuration using a shear-assisted processing and extrusion (ShAPE) machine (BOND Technology Inc), whose apparatus is schematically illustrated in Fig.1a. A rotating MP159 die, with two inward spiral grooves on its face, was employed for the powder extrusion [13]. The temperature was monitored using a K-type thermocouple embedded into the die 1 mm below the face of the die. During extrusion, the die rotating at 25 rpm was plunged toward the powder puck at a constant speed of 1 mm/min. The extrudate had a diameter of 2.54 mm, yielding an extrusion ratio (defined as the ratio of the cross-sectional area of the pre-compacted puck to the extrudate) of 100:1.

The copper extrudate was then sectioned transversely into rod samples, each having a segment length of 25.4 mm. Samples were wrapped with Zr foil (oxygen getter) and heat treated to the target temperatures separately (100°C, 200°C, 300°C, 400°C, 500°C, and 600°C) for 1 h in a Vulcan box furnace (Model 3-550), followed by water quenching. The densities and porosities of both extruded and heat-treated samples were measured by the Archimedes method in isopropanol. Samples were then mechanically ground and chemical-mechanically polished using colloidal silica media for hardness testing and electron microscopy. Microhardness testing was conducted using an FM-ARS9000 (Future-Tech Corp.) microhardness tester, with an indentation load of 50 g and a holding time of 12 s.

Scanning electron microscopy (SEM) was carried out using a Quanta 3D field-emission SEM (FEI/Thermo Fisher Scientific Inc.) to reveal the microstructure evolution. The transmission electron microscopy (TEM) sample from the extrudate was prepared by applying the focused ion beam (FIB) lift-out technique. TEM observation was conducted through a JEM-ARM200CF microscope (JEOL Ltd.) operated at 200 kV.

3. Results and Discussion

The temperature and force profiles during extrusion of powder A were recorded and are presented in Fig. 1b. The extrusion force peaked at 200 kN and dropped afterwards, dividing the extrusion into two regimes. The decline in force is believed to be a result of softening as deformation occurs at the higher homologous temperature of Cu. At ~450°C, the required flow stress to sustain deformation became lower than the applied stress, resulting in a force drop [14]. After this cross-over, the extrusion entered the 2nd processing regime until completion, resulting in a 340 mm long wire (Fig. 1c). The last-out ~170 mm (second half) of the extrudate from this regime was used for analysis in this study. Fig. 1d presents a cross-sectional overview of the extrudate, which appears to be well consolidated at low magnification. A magnified SEM micrograph in Fig. 1e, though, depicts submicron, spherical/equiaxed pores in the extrudate. They are uniformly distributed in the microstructure (the three-dimensional nature of their distribution is further corroborated by the side view in Fig. S1, enabled by FIB). The bright-field TEM micrograph in Fig. 1f reveals the fine grains and their interplay with the pores in the extrudate. The sharp grain boundary contrast and the growth twins in the grains (Fig. S2) suggest the friction-extrusion–processed microstructure is dictated by dynamic recrystallization and grain growth, consistent with early reports of the friction-extruded microstructure [14,15]. Notably, both intergranular (yellow arrows) and intragranular (white arrows) pores are observed, which is clearer and more discernable in the tilting movie of the specimen (Movie S1). The origin and the evolution of those pores at different temperatures are the central theme of this study.

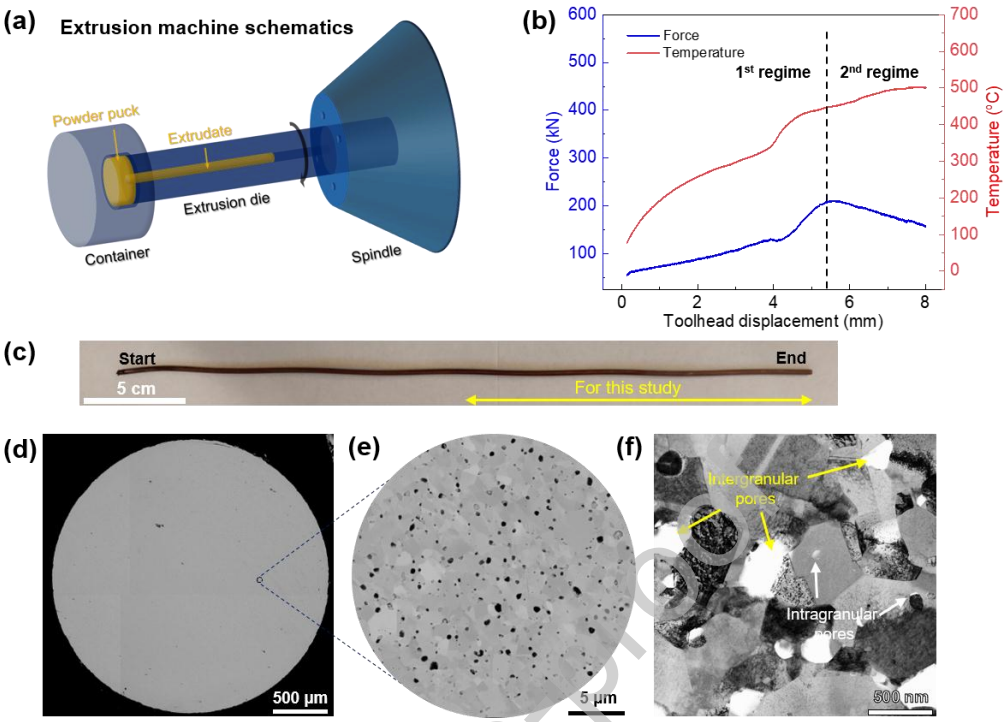

Figure 1. (a) Extrusion machine schematic showing the friction consolidation and extrusion apparatus; (b) key output processing parameters (force and temperature) as a function of the toolhead displacement during fabrication showing two distinctive regimes for extrusion; (c) the entire copper extrudate produced; (d) a backscatter electron image of the entire extrudate transverse section; (e) an increased magnification view revealing the submicron pores and their distribution; and (f) the bright-field TEM micrograph showing the pore structure and surrounding grain characteristics.

When heated at different temperatures for 1 h, the pore structure and grain structure underwent a remarkable evolution (Fig. 2). Based on microstructural characterization, density, and hardness measurements, the porosity evolution can be roughly divided into three stages. Below 300°C is *Stage I*, at which the pore structure remains relatively stable—both the almost equivalent diameter (Fig. 2b) and the spatial distribution (Fig. 2a1-a2) of pores almost remain unchanged. *Stage II* covers the temperature range from 400°C to 500°C, where the individual pores expand dramatically (Fig. 2a3), and the overall porosity reaches the peak of ~25% (Fig. 2c). Importantly, the transition from *Stage I* to *Stage II* is strikingly sharp—the overall percent porosity triples from 300°C to 400°C. At *Stage III*, large pores gradually shrink and disappear, skewing the pore size distribution toward reduced size at 700°C (Fig. 2b). As the temperature increases beyond 500–600°C (Fig. 2c), the overall porosity gradually declines. Additional plots of average pore size and number density are provided in Fig. S3, which signify the same trend. It is notable that most remnant pores at *Stage III* reside along the grain boundaries, which sheds light on the porosity evolution mechanism, as discussed later. The porosity evolution affects the hardness of samples. Hardness remains stable below 300°C, but drops significantly at 400°C, matching the sharp porosity transition from *Stage I* to *Stage II*. Above 500°C, hardness gradually increases, consistent with the porosity decline at *Stage III* at high temperatures. Nevertheless, the consolidation-induced hardening is also compensated by the loss of grain boundary strengthening due to the substantial grain growth at high temperatures. Consequently, it leads to only slight incremental increases in hardness. The observed

hardness evolution as a function of porosity is in agreement with the early reports on the relationship between strength and pore volume fraction in Cu [16,17].

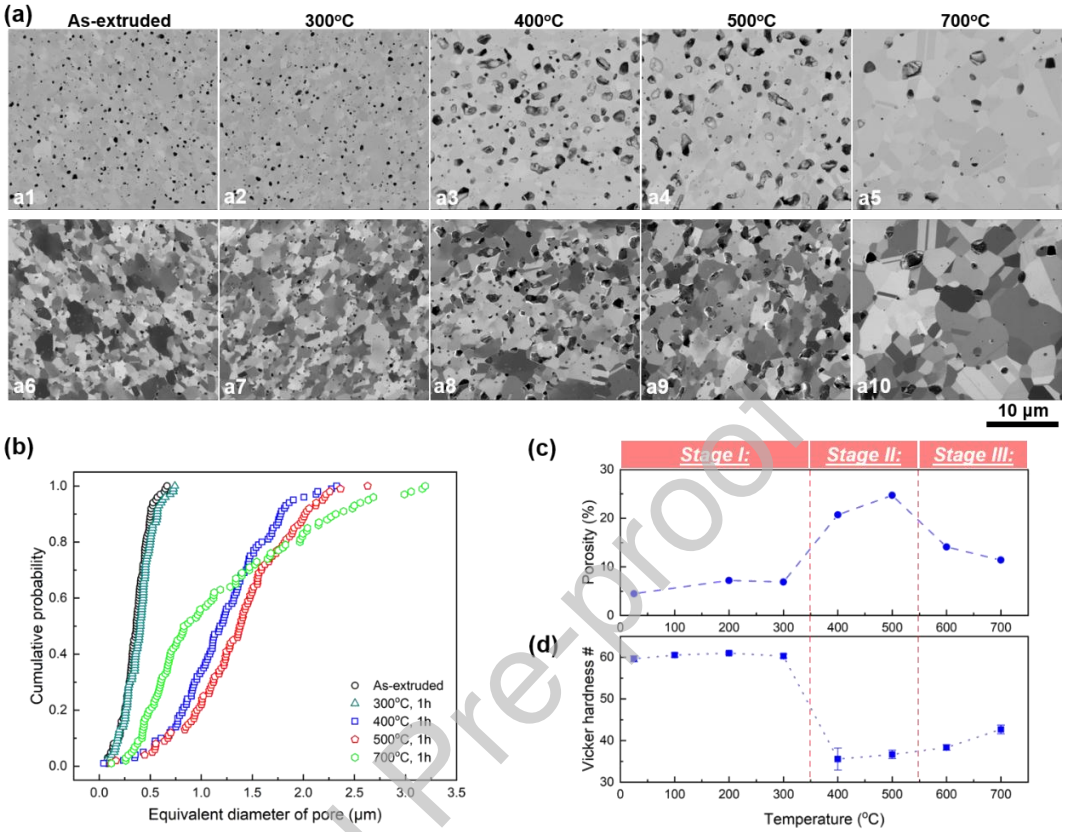

Figure 2. (a) Backscatter electron imaging (upper row: for pore structure) and ion channel contrast imaging (lower row: for grain structure) revealing microstructural comparisons under the extruded condition and after heat treatment to different temperatures. (Each column represents the data from the same location of the sample, and all images scaled equivalently.) (b) Cumulative probability plots of the measured pore size under different conditions; (c) porosity calculated from density measurement by the Archimedes method; and (d) Vickers hardness results of the samples under different conditions showing an abrupt drop that coincides with a porosity increase at 400°C followed by incremental increases past 500°C.

For the rest of the manuscript, we will address the origin of the pores and explore the underlying mechanisms of microstructural evolution as a function of heat-treating temperature. First, two sources of porosity were hypothesized based on the origin of the pores in the extrudate:

- One is from the feedstock powder, particularly the initial porosity induced by the trapped gas during the atomization process, which can be regarded as the internal source.
- The other is the entrapping gas during the powder consolidation and extrusion process, i.e., the external source. The neighbor but disjoint powder particles can be bonded under the stress and elevated temperatures during extrusion. The gas entrapped in the sealed space between those particles (see Fig. S4) will determine the initial porosity.

To investigate whether either or both sources are operative, powder B was extruded under the similar condition (Fig. 1b and Fig. S5) to enable a direct comparison. Fig. 3a and b demonstrate the cross-sectional micrographs of the two different powders—one has large-size particles and significant

submicron porosity (used in the main study) and the other exhibits a more dendritic morphology (irregular outlines in the cross section) and is composed of refined and pore-free particles. The respective microstructure and the density-determined porosity of each extrudate are provided in Fig. 3c and 3d. Both extrudates exhibit appreciable porosity, suggesting that both feedstock powders experienced incomplete consolidation (process-induced porosity). However, because the porous powders resulted in a nearly doubled porosity over the electrolytic powder (4.5% vs. 2.2%, respectively), this also reveals that porosity inherent to the feedstock material is also retained. In this way, we have demonstrated a method by which extrudate porosity can be tailored not only by heat treatment (Fig. 2) but also by careful consideration of precursor materials. This also suggests different feedstock materials could be potentially heat treated to incorporate various levels of porosity at the same temperature.

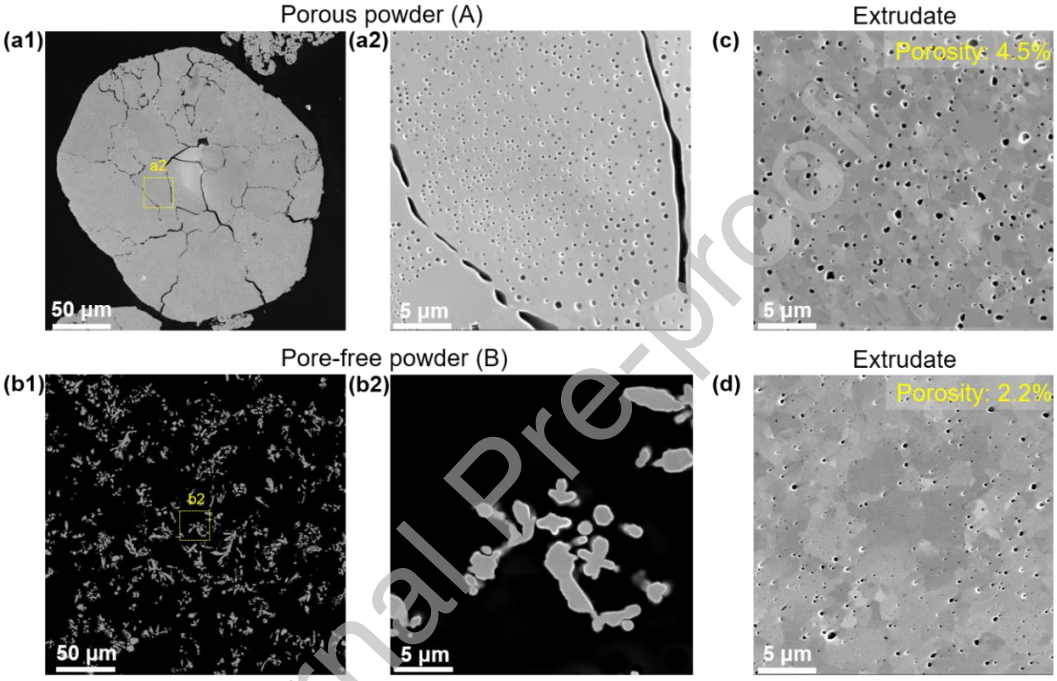

Figure 3. SEM observation of the porous, large-size feedstock powder before extrusion (a1-a2) and the resultant microstructure in the extrudate (c); SEM observation of the pore-free, fine-size feedstock powder before extrusion (b1-b2) and the resultant microstructure in the extrudate (d).

With regard to tailoring extrudate porosity by controlling porosity evolution during heat treatment, it is apparent that temperature does not simply influence the porosity in a continuous fashion. The trendlines first shown in Fig. 2 suggest that a transition in the driving force (as a function of temperature) controls pore evolution. Fig. 4a demonstrates the different mechanisms that govern the porosity evolution as the heat-treatment temperature rises. The rationale is based on the observed three-stage evolution and is anchored to the competition between the internal pore pressure, material strength, and sintering kinetics, as a function of temperature. From the ambient to the critical temperature (T_c), the internal pore pressure is lower than the material strength. Therefore, the pore structure is expected to be stable and produces the porosity plateau observed in *Stage I*. Internal pore pressure continues to increase while the material strength declines quickly as the temperature rises. Once T_c is reached, the pores start to expand by plastically deforming the surrounding metal matrix, which elucidates the porosity spike observed in *Stage II*. It should be noted that, in addition to yielding, creep also plays a vital role during this stage because of the increase in temperature and gas pressure [18]. Creep-induced pore expansion is most rapid in the early

period of heating because the internal pressure is initially high and drops rapidly as pores expand [10,19]. In this study, the crucial role of creep can be simply justified by the discrepancy between the measured porosity increment and the yielding-based prediction. Considering the gas condition at 300°C (condition 1), the internal pressure (p_1) should be close to, but should not exceed, the yield strength (σ_1) because 300°C is the highest temperature for a relative stable porosity, i.e., $p_1 < \sigma_1$. For 400°C (condition 2), the internal pressure (p_2) is presumably equivalent to the yield strength of the Cu matrix (σ_2) after pore expansion, i.e., $p_2 \approx \sigma_2$. Therefore, the pore volumes of these two statuses would follow the relationship below:

$$\frac{V_2}{V_1} = \frac{T_2}{T_1} \cdot \frac{p_1}{p_2} < \frac{T_2}{T_1} \cdot \frac{\sigma_1}{\sigma_2} \qquad (1)$$

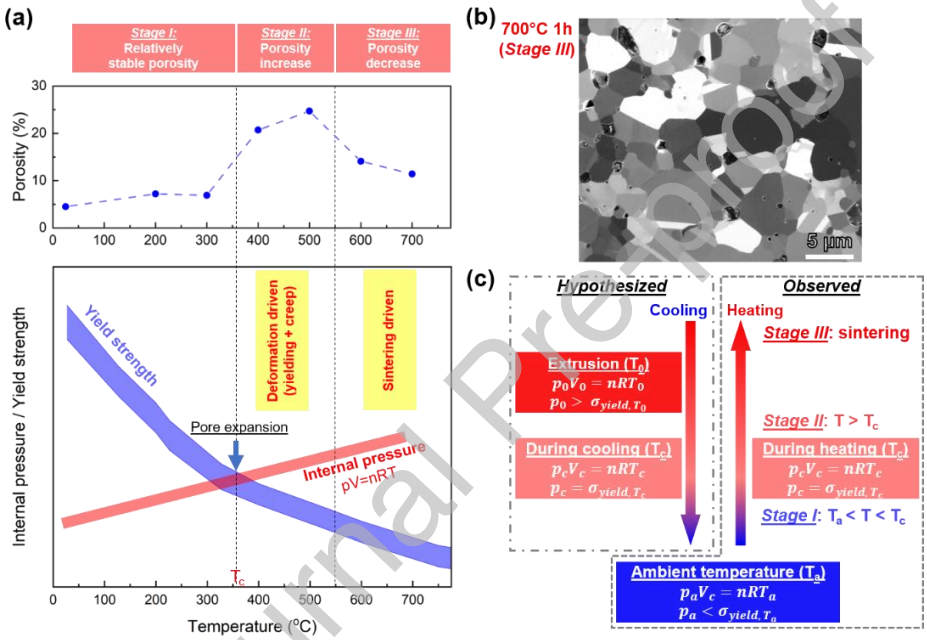

Figure 4. (a) Rationale of the three-stage evolution of porosity in the extrudate as the function of temperature for heating; (b) grain and pore structures after heat treatment at 700°C for 1 h, resembling the key microstructure characteristics on the intermediate/final stage of sintering; and (c) the relationship between the entrapped gas condition and the Cu matrix strength during the extrusion and cooling (hypothesis-based) as well as heating (observation-based) processes.

According to the temperature-dependence of Cu yield strength [20–22], the ceiling ratio of σ_1/σ_2 is no greater than 2. Thus, V_2/V_1 is expected smaller than 2.4 using Eq. (1). However, the measured porosity results reveal that the ratio of V_2/V_1 is closer to 4, much greater than the pore expansion-based value of 2.4 calculated from the yielding consideration alone. Hence, both yielding and creep contribute to the observed pore expansion observed in *Stage II*. Additionally, we also note other potential contributors to the porosity; for example, the collapse of the vacancies produced during extrusion deformation [23] and the grain boundary excess volume reduction after the significant grain growth [24]. However, the results of the detailed evaluations suggest both play minor roles, neither producing a pore volume greater than

0.1% (see Appendix S1 and S2). The contribution of all factors considered for *Stage II* is listed in Table 1, where yielding and creep are expected to dominate.

Table 1. Analysis of contribution to the porosity increase from 300°C to 400°C

Source for pore expansion	Contribution to the pore expansion
Deformation by yielding	< 60%
Deformation by creep	> 40%
Collapse of vacancies during extrusion deformation	~0.02%
Gain of excess volume from reduced grain boundary area during heating	~0.01%

Further increasing the temperature boosts the diffusion, thereby entering *Stage III* where the sintering process becomes pronounced. Interfacial energy reduction drives the shrinkage and closure of pores gradually via enhanced diffusion. During this process, remnant pores commonly reside at triple points or boundary junctions (Fig. 4b), consistent with the classical Coble's diffusion model for the intermediate/final stage of sintering [25]. Experimentally, the temperature triggering a significant reduction in porosity agrees well with the temperatures reported for direct sintering of Cu powders [26,27], lending further credence to the sintering-governed microstructural evolution at temperatures above 600°C.

The critical temperature (T_c) for the transition from *Stage I* to *Stage II* depends on the internal pore pressure in the extrudate at the ambient temperature based on the ideal gas law (see the Observed box in Fig. 4c). Naturally, this pressure results from the extrusion process, and its evolution can be rationally hypothesized in the left box of Fig. 4c. During the second regime of extrusion at T_0 (450~500°C in Fig. 1b), the entrapped gas resists the flow stress exerted on pores, regardless of the internal or external source. This resistance leads to an internal pressure (p_0) equivalent to the flow stress, which must be greater than the material yield strength ($\sigma_{\text{yield, } T_0}$) to enable extrusion. Following extrusion, pores tend to expand due to the gas pressure being temporarily higher than the material yield strength. However, as the temperature is reduced, the gas pressure drops, and the material yield strength increases simultaneously. Therefore, shortly after the extrusion, the porosity reaches its equilibrium value upon cooling from T_c to ambient temperature. This T_c is the same as the transition temperature from *Stage I* to *Stage II* during heating. The observed T_c during heating being slightly smaller than the extrusion temperature T_0 lends credence to this hypothesis for the extrusion and subsequent cooling process.

The findings of three-stage extrudate porosity evolution during heating have important implications for microstructural engineering in advanced manufacturing. First, the relatively wide porosity window during evolution (4~25%) provides a promising outlook for tailorable porosity in extrudates by tuning post-heating temperatures. Second, the extrusion parameters (temperature, flow stress, etc.) determine the starting porosity and internal pore pressure, thus strongly affecting the porosity evolution path. On the one hand, increasing the flow stress could lead to a high initial gas pressure and further increase the extreme porosity during heating, potentially opening a new avenue for solid-state foaming. On the other hand, increasing the extrusion temperature to that in *Stage III* could trigger effective sintering during the extrusion process and produce more consolidated extrudates (if the entrapped gas is highly diffusive).

4. Summary

To summarize, we studied the porosity evolution during heating of copper extrudates processed from powders by friction extrusion. We then observed and reported a three-stage pattern of pore evolution (steady-state, increasing, and ultimately decreasing) as a function of heat-treating temperatures. The

underlying mechanisms driving the three-stage evolution were discussed based on the internal pore pressure, material strength, and sintering kinetics, all as a function of temperature. The observation here is not anticipated to be limited to copper and may also prove applicable to other metallic materials in advanced manufacturing by direct powder extrusion.

Declaration of Competing Interest

The authors declare that they have no known competing financial interests or personal relationships that could have appeared to influence the work reported in this paper.

Acknowledgments

This research was supported by the Solid Phase Processing Science Initiative at the Pacific Northwest National Laboratory, USA. The authors are grateful to Anthony Guzman and Michael Blazon for their preparation of specimens for microstructural characterization, Mark Rhodes for his heat treatment of specimens, and Dr. Tianhao Wang for his insightful discussions. The Pacific Northwest National Laboratory is operated by Battelle for the U.S. Department of Energy under contract DE-AC06-76101830.

Reference

[1] L.-P. Lefebvre, J. Banhart, D.C. Dunand, Adv. Eng. Mater. 10 (2008) 775–787.

[2] M.A. Atwater, L.N. Guevara, K.A. Darling, M.A. Tschopp, Adv. Eng. Mater. 20 (2018) 1700766.

[3] R. Goodall, A. Mortensen, in: Phys. Metall., Elsevier, 2014, pp. 2399–2595.

[4] S. Leuders, M. Thöne, A. Riemer, T. Niendorf, T. Tröster, H.A. Richard, H.J. Maier, Int. J. Fatigue 48 (2013) 300–307.

[5] E. Brandl, U. Heckenberger, V. Holzinger, D. Buchbinder, Mater. Des. 34 (2012) 159–169.

[6] S.-J.L. Kang, in: Sintering, Elsevier, 2005, pp. 3–8.

[7] M.W. Kearns, P.A. Blenkinsop, A.C. Barber, T.W. Farthing, Met. Mater. Bury St Edmunds 3 (1987) 85–88.

[8] N.G.D. Murray, D.C. Dunand, Acta Mater. 52 (2004) 2269–2278.

[9] S.M.H. Hojjatzadeh, N.D. Parab, W. Yan, Q. Guo, L. Xiong, C. Zhao, M. Qu, L.I. Escano, X. Xiao, K. Fezzaa, W. Everhart, T. Sun, L. Chen, Nat. Commun. 10 (2019) 3088.

[10] S. Tammas-Williams, P.J. Withers, I. Todd, P.B. Prangnell, Scr. Mater. 122 (2016) 72–76.

[11] S. Whalen, M. Olszta, C. Roach, J. Darsell, D. Graff, Md. Reza-E-Rabby, T. Roosendaal, W. Daye, T. Pelletiers, S. Mathaudhu, N. Overman, Materialia 6 (2019) 100260.

[12] X. Li, W. Tang, A.P. Reynolds, W.A. Tayon, C.A. Brice, J. Mater. Process. Technol. 229 (2016) 191–198.

[13] N.R. Overman, S.A. Whalen, M.E. Bowden, M.J. Olszta, K. Kruska, T. Clark, E.L. Stevens, J.T. Darsell, V.V. Joshi, X. Jiang, K.F. Mattlin, S.N. Mathaudhu, Mater. Sci. Eng. A 701 (2017) 56–68.

[14] X. Li, N. Overman, T. Roosendaal, M. Olszta, C. Zhou, H. Wang, T. Perry, J. Schroth, G. Grant, JOM (2019).

[15] S. Whalen, N. Overman, V. Joshi, T. Varga, D. Graff, C. Lavender, Mater. Sci. Eng. A 755 (2019) 278–288.

[16] A.E. Simone, L.J. Gibson, Acta Mater. 44 (1996) 1437–1447.

[17] S.K. Hyun, K. Murakami, H. Nakajima, Mater. Sci. Eng. A 299 (2001) 241–248.

[18] B. Wilshire, A.J. Battenbough, Mater. Sci. Eng. A 443 (2007) 156–166.

[19] N.G.D. Murray, D.C. Dunand, Acta Mater. 52 (2004) 2279–2291.

[20] R.P. Carreker, W.R. Hibbard, Acta Metall. 1 (1953) 654–663.

[21] T.J. Miller, S.J. Zinkle, B.A. Chin, J. Nucl. Mater. 179–181 (1991) 263–266.

[22] T. Suo, Y. Li, K. Xie, F. Zhao, K. Zhang, Y. Liu, Mater. Sci. Eng. A 527 (2010) 5766–5772.

[23] M. Wegner, J. Leuthold, M. Peterlechner, D. Setman, M. Zehetbauer, R. Pippan, S.V. Divinski, G. Wilde, J. Appl. Phys. 114 (2013) 183509.

[24] E.-M. Steyskal, B. Oberdorfer, W. Sprengel, M. Zehetbauer, R. Pippan, R. Würschum, Phys. Rev. Lett. 108 (2012) 055504.

[25] R.L. Coble, J. Appl. Phys. 32 (1961) 787–792.

[26] Y.-J. Lin, K.-S. Hwang, Mater. Trans. 51 (2010) 2251–2258.

[27] R. Collet, S. le Gallet, F. Charlot, S. Lay, J.M. Chaix, F. Bernard, Mater. Chem. Phys. 173 (2016) 498–507.